Power law correlations for gas/liquid flow in a flexible pipeline simulating terrain variation

By Clara Mata and Jany C. Vielma

PDVSA-Intevep, Los Teques 1201, Edo. Miranda, Venezuela

Daniel D. Joseph

Aerospace Engineering and Mechanics, Univ. of Minnesota, Minneapolis, MN 55455

June 2002

Abstract

The problem of prediction of the pressure drop in gas-liquid pipelines in oil reservoir applications are compounded by the fact that such pipelines generally are not straight; they go up and down, this way and that. To simulate such terrain variations we built a flexible tygon tube pipeline. This paper reports the results of experiments in this pipeline. In the general study of gas-liquid flow, flow regime transitions are identified and then pressure gradient models for each flow regime are derived. These models are used in simulators to guide field operations in gas-liquid pipelines; the models are not accurate, they are expensive to implement and certainly not suitable for pipelines in complicated configurations in which different flow regimes are simultaneously present. An alternative is to get the pressure gradient and holdup predictions directly from a systematic processing of real data for correlations; this procedure is used here. We processed data from gas/liquid flows in our flexible flow loop using mineral oil and air for four different elevation profiles. We found correlations for liquid holdup and friction factors as a function of the liquid Reynolds number $\mathrm{Re}_L = U_L\, D/D_L$ and flow rate fraction $\lambda = Q_G/(Q_G+Q_L)$ in each configuration. An overall correlation for the holdup and friction factor using all the data from all four elevation profiles was also obtained. The overall correlations are of course less accurate but are proposed for the typical situation in which the elevation profile for a particular pipeline is not known or is not available.

The holdup correlations are in the form

$$h_L = e\,\mathrm{Re}^r (1-\lambda)^{l\,\mathrm{Re}^s} \qquad (1)$$

This is a composition of power laws with prefactor e in which the exponent of $(1-\lambda)$ is also a power law with prefactor l. The friction factor correlations are in the form

$$f_M = h_L^{\,p}(1-\lambda)^n\, 16/\mathrm{Re}_M^{\,m} \qquad (2)$$

which is a tri-power law in h_L, $(1-\lambda)$ and the *mixture* Reynolds number Re_M. For the

horizontal pipeline the classical friction factor result for laminar flow $f_M = 16/\mathrm{Re}_M$ $(p,m,n) = (0,1,1)$ is very nearly satisfied with the caveat that the mixture superficial velocity $U_M = U_G + U_L$ must be used. For the other elevation profiles, and overall, the exponents and prefactors are different. The presence of the holdup in the correlations (2) shows that the friction factor depends on the holdup; we found that this holdup factor was effective in reducing scatter. Two flows with the same Re_M and $(1-\lambda)$ will give rise to different friction factors if the holdups are different.

The errors in the predicted values of holdup using correlations are typically less than 5% with maximum errors of 15% for the overall correlations. For the friction factor correlations the errors are typically less than 15% with maximum errors in the neighborhood of 25% when correlations are taken over all data. These errors are much smaller than errors typical for models even when there are no terrain variations.

1 Introduction

Multiphase flow through pipes and annular ducts is an important technical subject in the oil industry. Detailed knowledge of this kind of flow is fundamental for the oil production system's proper design. Multiphase flow systems are highly complex and many aspects of their behavior are not well understood today. This lack of knowledge is especially critical in the case of heavy/extra-heavy oils.

In the study of gas-heavy oil flow, emphasis has been made in the general study of gas-liquid flow in which flow regime transitions are identified and then pressure gradient models for each flow regime are applied. These studies have led the multiphase flow community to develop of complicated and expensive simulators.

In this work we follow a different method, the method of correlations, which eschews models relying instead on systematic processing of real data to obtain formulas, analytic expressions, relating relevant dimensionless parameters, to predict future performance. In this application, we collected and then arranged physical and experimental data in the columns of a spread sheet. The data was then composed into dimensionless groups believed relevant and tested for power law correlations by plotting in log-log plots, all by a click of the mouse. This is and old, tried and true, method given new life by the power of digital technology and systematic procedures for processing data.

Our enthusiasm for correlations has to do with the surprising emergence of correlations from the simplest kind of post-processing of numerical experiments for lift of single particles (Patankar, Huang, Ko and Joseph, 2001a) and many particles in slurries (Patankar, Ko, Choi and Joseph, 2001b). The procedure these authors follow is to plot the results of simulations in log-log plots of the relevant variables. If the choice is good these plots come up as straight lines giving rise to power laws. For example, a single particle will lift off in Poiseuille flow at a certain Reynolds number Re, given a settling number R_G (Patankar et. al. 2001a). When Re and R_G lie on the locus of $\mathrm{Re} = aR_G^{\,n}$ with intercept a and slope n in the log-log plot. The straight lines in the simulation data are impressively straight; correlations from simulations were generated for single particle lift-off in non-Newtonian fluids (Ko, Patankar and Joseph 2002), for the bed expansion of slurries (Choi and Joseph 2001, and Patankar 2001b) and fluidized beds (Pan, Joseph, Glowinski and Sarin, 2002).

Power laws emerge when only two variables are at play; when there are three variables or more, say Re, R_G and α, we would fix α, find $\mathrm{Re} = a(\alpha) R_G{}^{n(\alpha)}$ and seek analytical expressions for $a(\alpha)$ and $n(\alpha)$. As far as we know, there are no published studies of pressure drop in pipelines with terrain variation modeled by our flexible pipeline.

It frequently happens that one sees power laws separated by transition regions. This is the case for the Richardson-Zaki correlation (Pan et. al. 2002); it has one power law relating the fluidization velocity to the solids fraction at low Reynolds numbers, and another at high Reynolds numbers, with a transition conveniently described by a logistic dose curve (Patankar et al 2001b), in between.

In the application to real experiments on bed transport of slurries studied by Wang, Joseph, Patankar, Conway and Barree (2002), five parameters are at play. They find correlations as a composition of *bi-power laws* in the proppant and fluid Reynolds numbers with exponents and prefactors expressed as logarithmic functions of dimensionless sedimentation numbers.

The method of correlations has a more or less universal applicability to data sets for all sorts of physical processes. It can be said that 'the secrets are in the data' and that correlations of data are a discipline of the researcher's imagination.

2 Power Law Correlations

We studied gas/liquid flow in a flexible flow loop (1" diameter and ~12m long) using mineral oil (130 cP at 25 °C) and air. Four different geometrical configurations were used. Given the air flow rate Q_G and the liquid flow rate Q_L, pressure gradient (ΔP), temperature (T) and average liquid hold up (h_L) were measured. We fit data with power law correlations of the form (1) and (2) where the gas and liquid superficial velocities are given by

$$U_G = \frac{4Q_G}{\pi D^2} \text{ and } U_L = \frac{4Q_L}{\pi D^2} \tag{3}$$

where D is the pipe diameter. The mixture velocity is $U_M = U_G + U_L$; the liquid flow rate fraction is

$$1 - \lambda = U_L / U_M \,. \tag{4}$$

The mixture Fanning friction factor is

$$f_M = \frac{\tau_w}{\frac{1}{2}\rho_L U_M^2}, \quad \tau_w = \left(\frac{\Delta P}{L}\right)\frac{D}{4} \tag{5}$$

where ρ_L is liquid density, τ_w is the wall shear stress and $\Delta P/L$ is the pressure gradient. The mixture Reynolds number Re_M is related to the liquid Reynolds number Re_L by

$$\mathrm{Re}_M = \frac{U_M D}{v_L} = \frac{U_L D}{v_L(1-\lambda)} = \frac{\mathrm{Re}_L}{1-\lambda}. \tag{6}$$

The three parameters Re_M, Re_L and λ are not independent. The correlations to be obtained are ultimately determined by two-dimensionless parameters chosen from the above three.

3 Experimental Set up

Figure 1 shows a schematic of our flexible gas/liquid flow loop. In figure 1(a) four sections are indicated: Air injection, liquid injection, by pass and test sections. The test section is made of a 1-in. diameter, and 12m and 12.8m long tygon tubes, which allowed us to study four different elevation profiles. This flow loop is automatically controlled. Pressure transducers (PT, DPT), temperatures transducers (TT), and fast closing valves (VCR) are also indicated. Liquid flow is measured with a flow meter (FT) and airflow is measured using an orifice plate. A gear pump (P) is used to circulate the liquid. Figure 1(b) shows the studied geometrical configurations. The actual length of the flow loop for the horizontal configuration is L = 12m. For the other three elevation configurations the test section length is L = 12.8m; the amplitudes and wavelength for these three configurations are given in the caption for figure 1.

Here follows a brief description of the experimental procedure. Mineral oil from the tank is circulated using a gear pump. Compressed air is injected into the system at the mixing point indicated in figure 1(a). The liquid flow rate Q_L is measured with a Micromotion flow meter. The air flow rate Q_G is measured by means of an orifice plate associated to a differential pressure transducer (DPT). The gas/liquid mixture then enters to the test section and it is finally separated at the tank. The pressure drop ΔP at the test section (of length $L \cong 12\mathrm{m}$) is measured once stable conditions are reached. Then the fast closing valves are simultaneously closed, while the mixture flow is diverted through the bypass section.

The average liquid hold up h_L is defined as follows:

$$h_L = \frac{V_L}{V_T} \tag{7}$$

where V_L is the volume of oil collected between fast closing valves in the test section. V_T is average volume of oil collected the same way after all the tests carried out with oil alone.

The oil density and viscosity were measured as a function of the temperature and the temperature was monitored in each experiment. The flow loop was calibrated using oil alone for each of the four configurations in figure 1 (b). The calibration results are presented in plots of the liquid Fanning friction factor f_L vs. liquid Reynolds number Re_L in figure 2. The experimental data for oil alone fits the theoretical value $f_L = 16/\mathrm{Re}_L$. However, to get the best fit we adjusted the diameter away from the nominal value $D = 0.0254$m of tygon tube; the adjusted diameters are $D = 0.0253$m for the case **A**, and $D = 0.0258$m for the case **B, C** and **D**. Obviously the tygon tube in elevation configurations would not be expected to retain the nominal diameter.

4 Experimental procedure and flow types

Four sets of experiments, one set for each of four elevation configurations shown in figure 1(b), were carried out. In these experiments the volume flow rates (Q_L, Q_G) for liquid and gas are prescribed; superficial velocities $(U_L, U_G) = (Q_L, Q_G)/\pi D^2$ are used to form dimensionless numbers. For each (Q_L, Q_G) the pressure gradient $\Delta P/L$, temperature T and average liquid holdup h_L were measured.

Figure 3 shows typical conditions in the plane of superficial velocities under which the air-oil experiments were conducted. Experiments carried out in a larger tube ($D = 2$ in.) for this oil-air system identified transitions from slug flow to dispersed bubble flow when the liquid velocity is large $U_L > 10$ m/s at moderate gas velocities. Annular flows occur when the gas velocity is very large and turbulent; slugs cannot be moved so fast and the gas pokes through. For small liquid flow rates with gas velocities not too large, stratified and wavy stratified flows appear.

In the horizontal tygon tube configuration A, slug flow and only slug flow was observed (figure 4). The flow there, with possible exception of incipient turbulence at the highest gas flow, was laminar. The appearance of incipient turbulence at the highest gas flow rate can also be identified in the friction factor vs. Reynolds number plots for the elevated configurations B, C and D. The flow type in the elevated configurations are mixed (figure 5) with stratified flow emerging on downward facing slopes. In general, flow regimes are separated by extensive regions of transitions. Mixtures of flow regimes are probably typical for pipelines with elevation profiles.

5 Processing and presentation of data

Data for holdup and friction factors are processed and presented in log-log plots in a search for power laws. Two parameters are plotted, the others are held fixed. If the two parameters give rise to a straight line, we may identify a slope and intercept corresponding to the power and prefactor of a power law. The power and prefactor depends on the parameters which were held constant in the power law search. The powers and prefactors are themselves processed for power laws, or otherwise, by plotting them against parameters originally fixed, which in the present case is the liquid Reynolds number. This leads to the composition of power laws in equations (1) and (2) of the abstract.

The friction factor plots corresponding to (2) in the abstract are constructed in a similar fashion and lead to a tri-power law in which the holdup is a factor.

We present log-log plots for holdup and friction factors for each of the four elevation profiles and overall and obtain power laws for each case, showing details.

The details are presented as a paradigm for finding power laws for real applications. The accuracy of the results is assessed by correlation coefficients σ^2 given for each log-log plot and by comparing predicted vs. experimental values also in log-log plots. The accuracy is satisfactory, even good, but the data from tygon tubes experiments is sparse and more needs to be done. Ultimately we should like to construct a database for all published gas/liquid pipelines, together with field data. In the present experiments it is possible that the scatter is less than what would be encountered in turbulent flow.

6 Holdup correlations

Log-log plots for $h_L = d(1-\lambda)^q$ are presented in figures 6—18 for different values of Q_L (Q_G is then determined $\lambda = Q_G /(Q_G + Q_L)$). The Reynolds $\mathrm{Re}_L = U_L D/\nu = Q_L D/\nu_L \pi D^2$ is then computed and power laws in powers of Re_L for d and q emerge (figures 7, 10, 13, 16) for the prefactors e and l and exponents r and s in (1). The prefactors $\bar{e}$ and $\bar{l}$ and exponents $\bar{r}$ and $\bar{s}$ in figure 18 are obtained from processing all of the data (called ALL) from all four configurations as if there were no differences between them. The results are given in tables 1 and 2. Errors are given in figures 8, 11, 14, 17 and 19. The errors are typically less than 5% with larger errors for low Q_L, short slugs separated by long intervals of stratified flow. Of course, the errors are greater (figure 19) for the overall correlation ALL in table 2.

7 Friction factor vs. Reynolds number correlations

These correlations are given graphically in figures 20 through 33. The goal is to determine the exponents for the tri-power law (2) giving f_M defined by $f_M = h_L^P(1-\lambda)^n 16/\mathrm{Re}_M^m$ as a function of Re_M, 1-λ and h_L (table 3).

8 Concluding remarks

The aim of the present effort is to promote the old tried and true method of correlations for obtaining predictive power law formulas for the response of multiphase flow systems by systematic interrogation of real data. Our application to gas-liquid flows in flexible pipelines which can be used to simulate terrain variations is important for the prediction of real pipelines in which many flow regimes are simultaneously present. We have shown how to create such power laws, using log-log plots sequentially first for power laws for holdup as a function of the liquid flow rate fraction, then for the prefactors and exponents of the resulting correlations. The errors in such correlations are uniformly small with larger errors for small liquid flow rates in which the stratified flow between slugs is more important. Pipelines with terrain elevation always develop a stratified portion on the downslope. The flow regimes are mixed in such lines and the predicted response, holdup and friction factors are beyond the present capability of mechanistic models. The friction factor correlations are all for laminar flow regimes in which $16/\mathrm{Re}_M$ is critical, with the caveat that the $\mathrm{Re}_M = U_M d/\nu_L$ depends on the mixture velocity and the liquid viscosity. Correlations for the friction factor, which do not account for holdup, are not accurate; the errors are large and different friction factors for the same Re_M are observed. Accounting for the holdup in the friction factor correlations greatly improves the accuracy and reduces scatter. The selection of relevant correlation parameters, and the methods of processing them are elements in the "tool box" for correlations. The potential for correlations is greatly enhanced by the power of computers and storage. The "tool box" can be viewed the "software" for this and it too has a great potential for development.

The results presented here are a paradigm for processing data in gas-liquid flow lines. To get definitive results, more data is required; data from the tygon tube, from the literature and from field operations. In particular, the difference in results for different elevation profiles can be correlated with as-yet-to-be-determined parameters which characterize the difference. We believe that the best predictive formulas for multiphase flow lines will arise from correlations as is true in the case of Moody diagrams for uniphase flows.

Acknowledgement

We are very thankful to Marcos Marcano, Guillermo Lombano, Victor Terán and Ramón Cabello for their valuable help in the design of the data acquisition system, set up, calibration and operation of the flow loop. The work of D.D. Joseph was supported by the Engineering Research Program of the Office of Basic Energy Sciences at the DOE, and under an NSF/GOALI grant from the division of Chemical Transport Systems.

References

Choi, H. G., D. D. Joseph, (2001). Fluidization by lift of 300 circular particles in plane Poiseuille flow by direct numerical simulation, *J. Fluid Mech.*, **438**, 101-128.

Ko, T., N. A. Patankar and D. D. Joseph (2002). Lift-off of a single particle in an Oldroyd-B fluid, *Int. J. Multiphase Fluids*, submitted.

Pan, T. W., D. D. Joseph, R. Bai, R. Glowinski and V. Sarin (2002). Fluidization of 1024 spheres: simulation and experiments, *J. Fluid Mech*., **451**, 169-191

Patankar, N. A., P. Y. Huang, T. Ko and D. D. Joseph (2001a). Lift-off of a single particle in Newtonian and viscoelastic fluids by direct numerical simulation, *J. Fluid Mech*., **438**, 67-100.

Patankar, N. A., T. Ko, H. G. Choi and D. D. Joseph (2001b). A correlation for the lift-off of many particles in plane Poiseuille flow of Newtonian fluids, *J. Fluid Mech.*, **445**, 55-76.

Wang, J., D. D. Joseph, N. A Patankar, M. Conway and R. D. Barree, (2002). Bi-power law correlations for sediment transport in pressure driven channel flow, *Int. J. Multiphase Fluids*, submitted.

Table 1. Parameters e, r, l and s plus correlation factor σ^2 for data presented in figures 6, 9, 12 and 15, which obey the following power law expression: $h_L = d(\mathrm{Re}_L)(1-\lambda)^{q(\mathrm{Re}_L)}$, where $d(\mathrm{Re}_L) = e\,\mathrm{Re}_L^{\,r}$ and $q(\mathrm{Re}_L) = l\,\mathrm{Re}_L^{\,s}$.

Configuration	*e*	*r*	σ^2 for $d(\mathrm{Re}_L)$	*l*	*s*	σ^2 for $q(\mathrm{Re}_L)$
A (Horizontal)	0.5856	0.0979	0.9928	0.1581	0.1672	0.9932
B	0.4367	0.1459	0.9591	0.1712	0.1342	0.5708
C	0.4241	0.1505	0.9899	0.1602	0.129	0.9756
D	0.3716	0.1748	0.9670	0.0571	0.3429	0.9360

Table 2. ALL data: parameters $\bar{e}$, $\bar{r}$, $\bar{l}$ and $\bar{s}$ plus correlation factor σ^2 for data presented in figure 18, which obey the following power law expression: $h_L = \bar{d}(\mathrm{Re}_L)(1-\lambda)^{\bar{q}(\mathrm{Re}_L)}$, where $\bar{d}(\mathrm{Re}_L) = \bar{e}\,\mathrm{Re}_L^{\,\bar{r}}$ and $\bar{q}(\mathrm{Re}_L) = \bar{l}\,\mathrm{Re}_L^{\,\bar{s}}$.

$\bar{e}$	$\bar{r}$	σ^2 for $\bar{d}(\mathrm{Re}_L)$	$\bar{l}$	$\bar{s}$	σ^2 for $\bar{q}(\mathrm{Re}_L)$
0.4474	0.1415	0.8595	0.1213	0.1978	0.6415

Table 3. Parameters n, m and p plus correlation factor σ^2 for fittings and data presented in figures 21, 24, 27, 31 and 32.

Configuration	*n*	*m*	*p*	σ^2
A (Horizontal)	1.119	0.964	-0.103	0.764
B	1.519	1.025	-1.892	0.554
C	1.516	1.025	-1.823	0.599
D	1.073	1.015	-1.101	0.554
ALL	0.7821	1.003	0.024	0.589

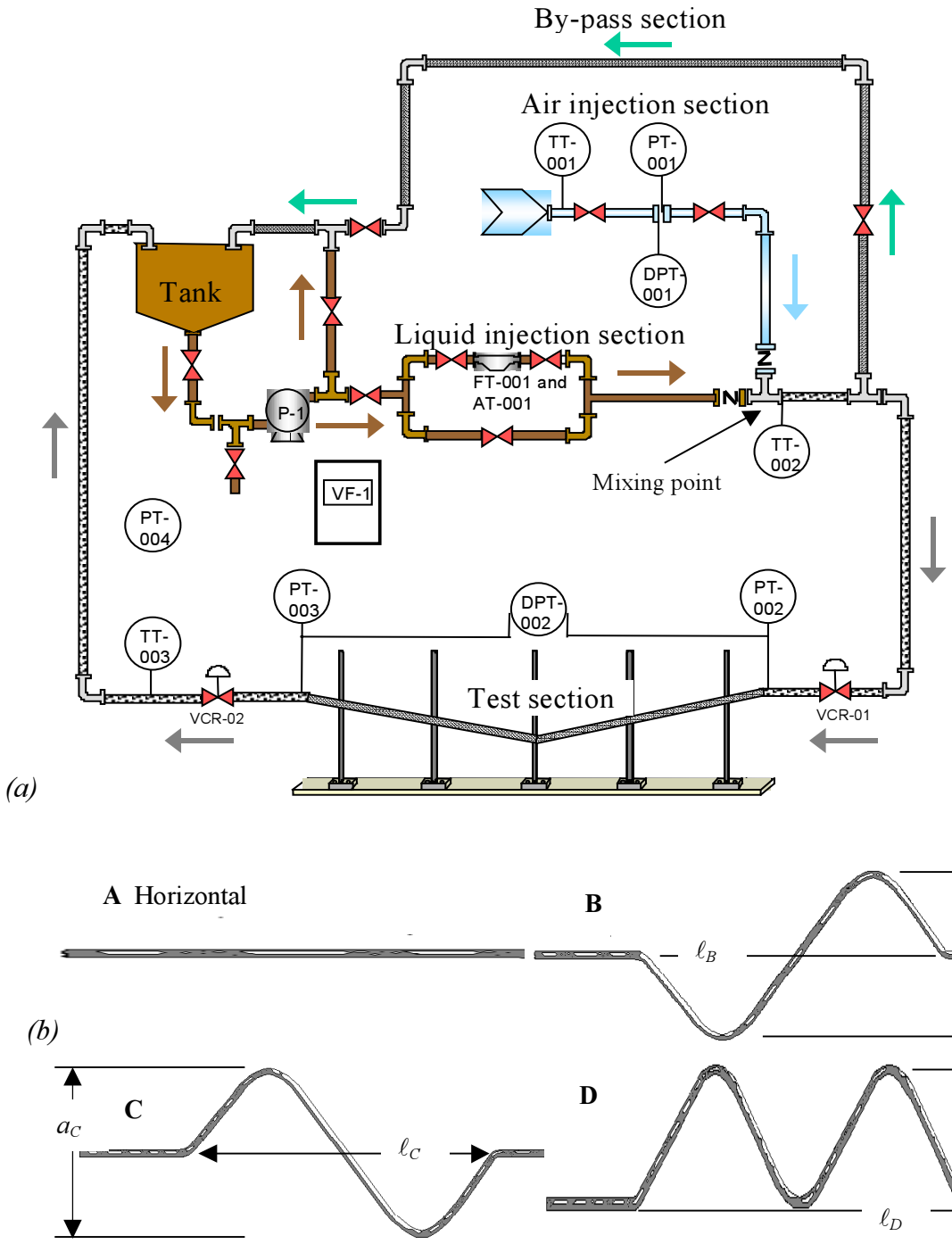

Figure 1. Flexible gas/liquid flow loop. (a) Schematics. Four sections are indicated: air injection, liquid injection, by pass and test section. This flow loop is automatically controlled. Pressure transducers (PT, DPT), temperatures transducers (TT), and fast closing valves (VCR) are indicated. Liquid flow is measured with a flow meter (FT) and air flow is measured using an orifice plate. A gear pump (P) is used to circulate the liquid. (b) Parameters of the four elevation configurations (l_B, l_C, l_D) = 0.8m, (a_B, a_C) = 1.8m and (a_D) = 0.9m.

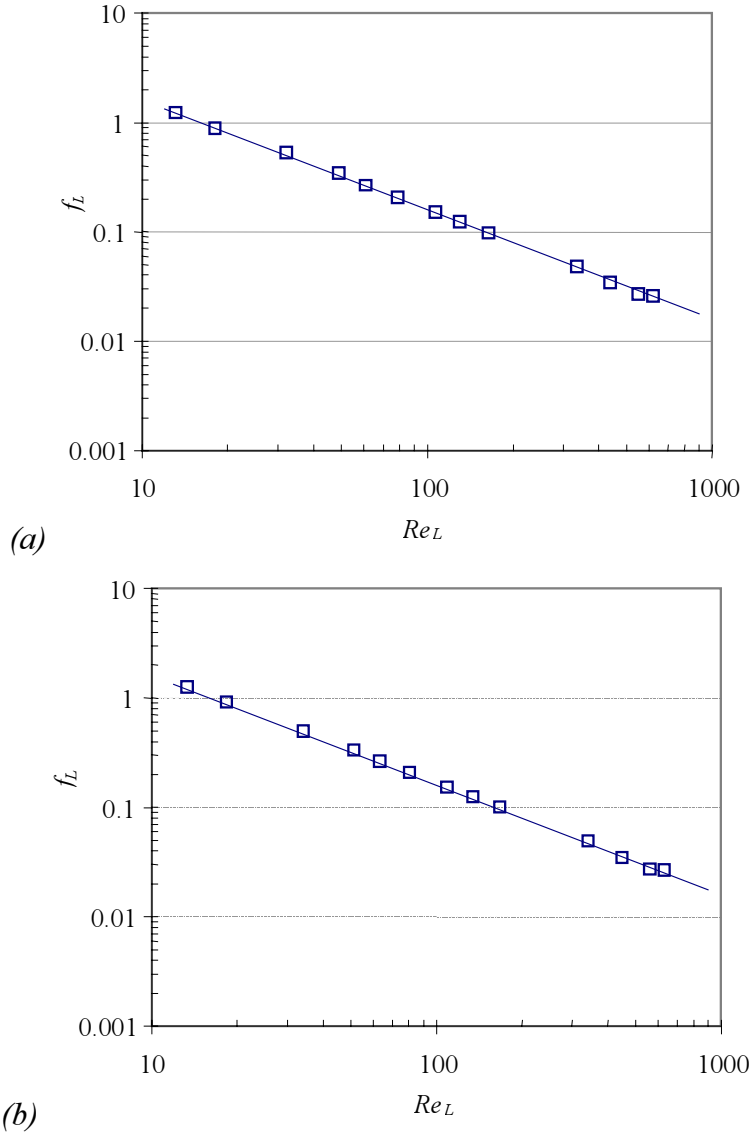

Figure 2. *Liquid Fanning friction factor f_L vs. liquid Reynolds number* Re_L *for experimental data obtained running oil alone in the tygon tube flow loop.*

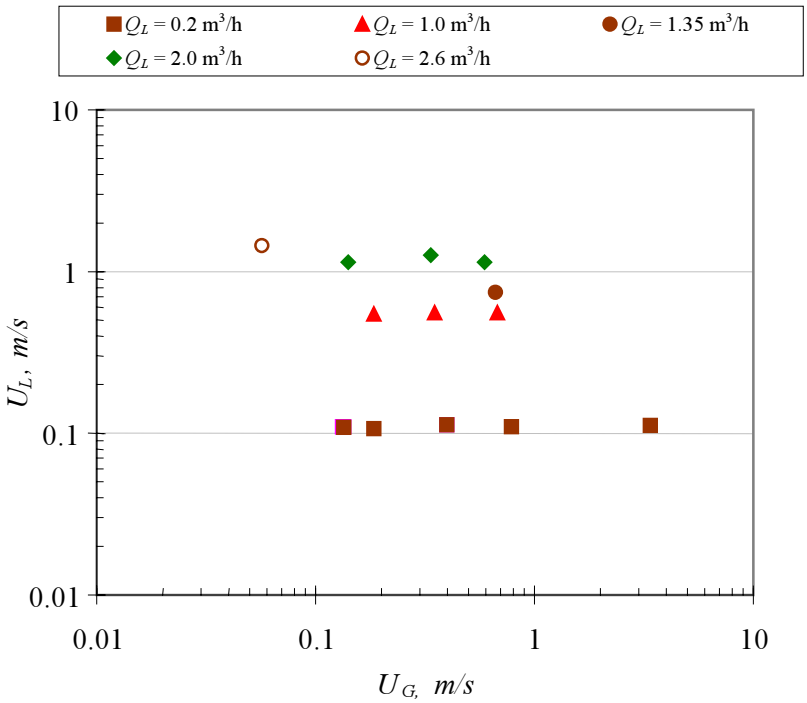

Figure 3. Typical experimental matrix of tests (liquid superficial velocity vs. gas superficial velocity) carried out in the tygon tube flow loop, running air and oil (130 cP at 25 ℃). Different liquid flow rates Q_L *are identified. The gas Reynolds number* $R_G = U_G D/\nu_G$ *was greater than 2300 for the largest gas velocity and was believed to be turbulent. The other tests were in laminar flow which could be identified as a slug flow in the horizontal configuration* ***A*** *and a mixed slug and stratified flow in the three other configurations* ***B***, ***C***, *and* ***D***.

(a)

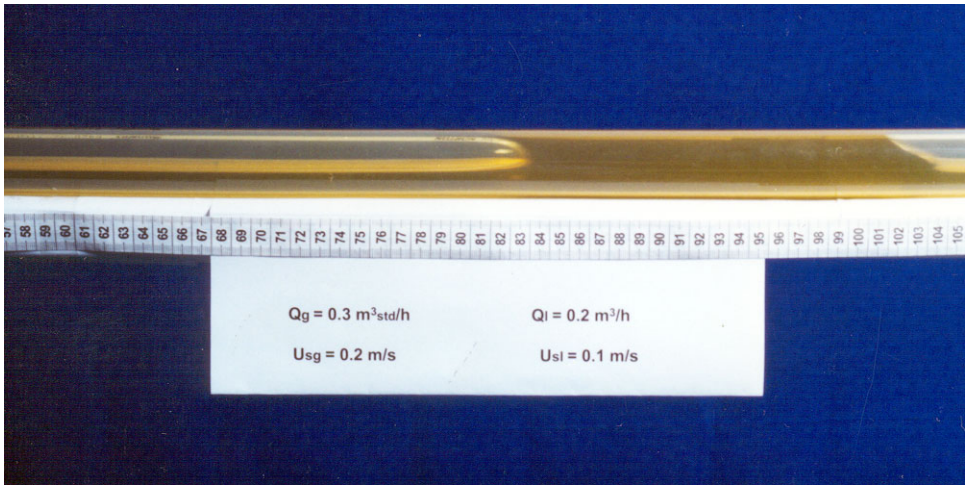

(b)

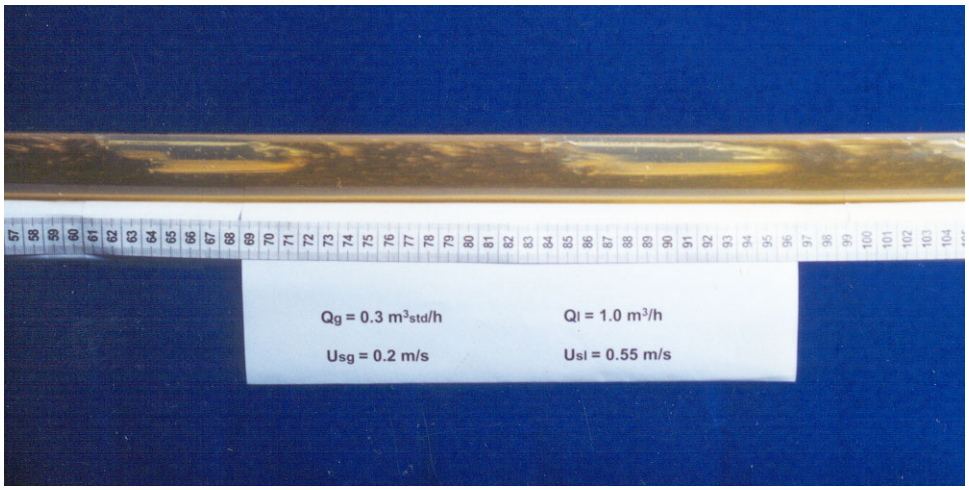

Figure 4. Pictures taken for a fixed gas flow rate, Q_G = 0.3 m^3/s, and two different liquid flow rates: (a) Q_L = 0.2 m^3/s and (b) Q_L = 1.0 m^3/s (b); in the tygon tube flow loop, using the horizontal configuration. In both cases slug flow is observed.

(a)

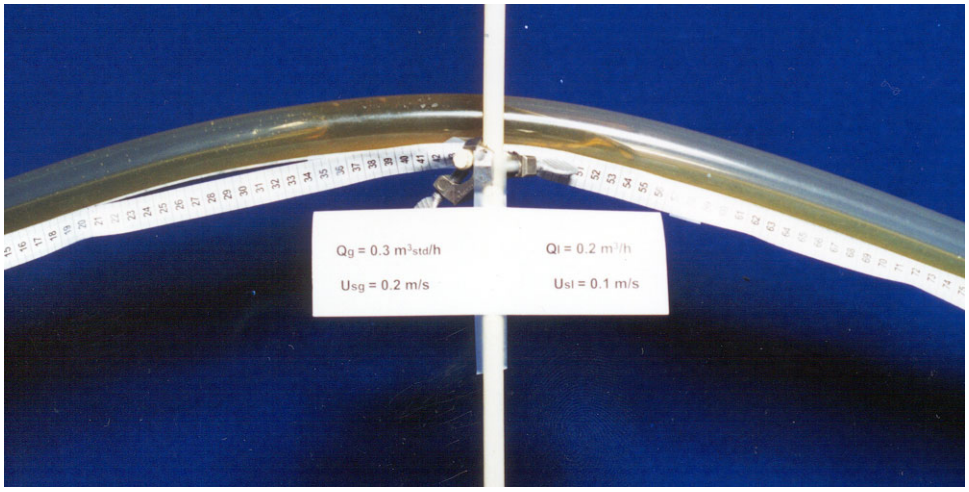

(b)

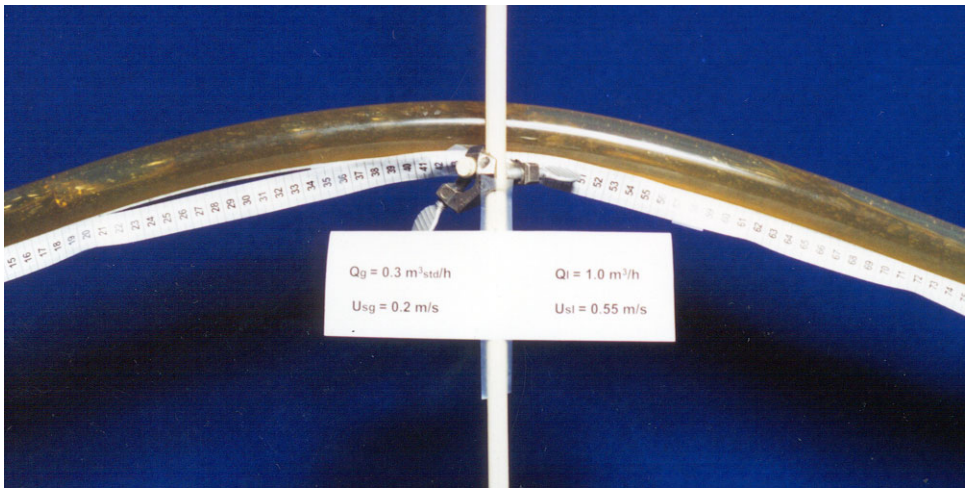

*Figure 5. Pictures taken for a fixed gas flow rate, $Q_G = 0.3\ m^3/s$, and two different liquid flow rates: (a) $Q_L = 0.2\ m^3/s$ and (b) $Q_L = 1.0\ m^3/s$; in the tygon tube flow loop, using the **D** configuration. In figure 5(a) Slug flow is observed for upward flow, and stratified flow is observed in downward flow. In figure 5(b) slug flow is observed for upward and downward flows.*

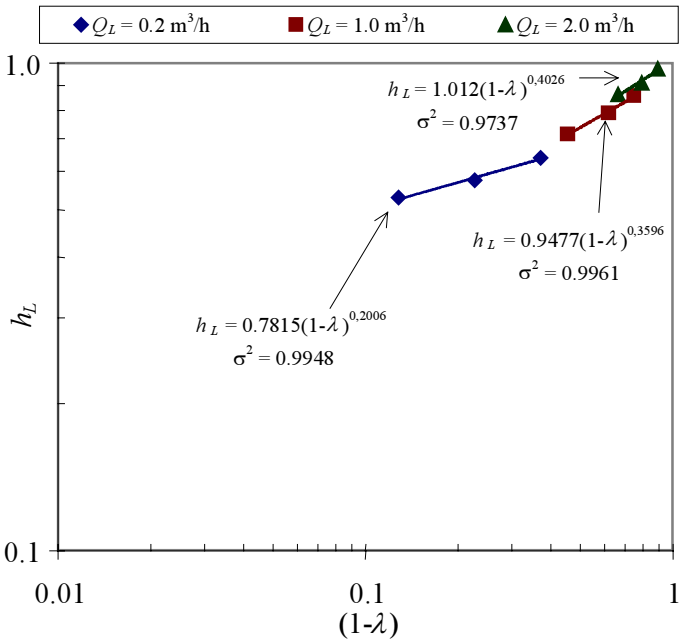

*Figure 6. Configuration **A**: Liquid holdup h_L vs. the flow rate ratio $(1-\lambda)$, for different liquid flow rates Q_L running air and oil in the tygon tube flow loop. To each liquid flow rate Q_L corresponds a liquid Reynolds number Re_L. A power law correlation of the form $h_L = d(1-\lambda)^q$ is obtained for each Re_L. The correlation coefficient is denoted by σ^2.*

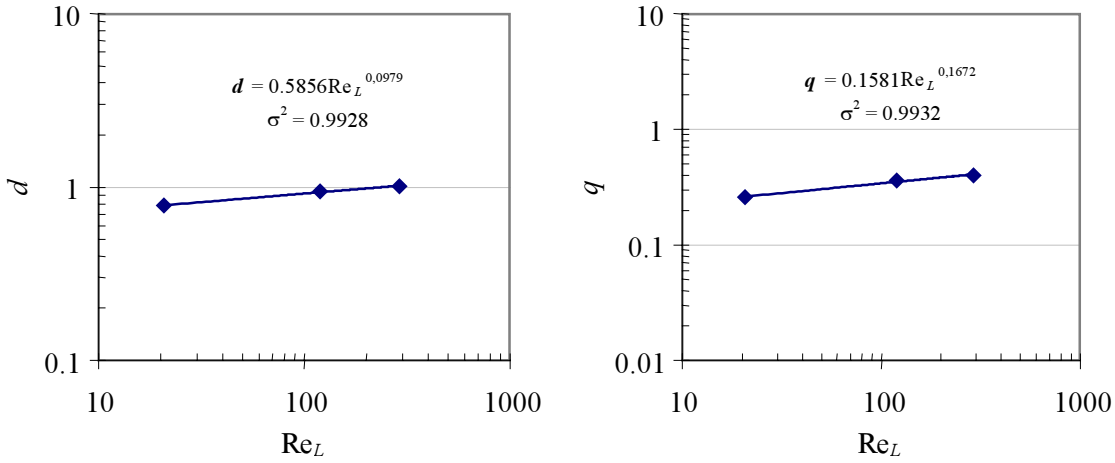

*Figure 7. Configuration **A**: Prefactor d and exponent q corresponding to the experimental data and fittings presented in figure 6 as a function of Re_L. Best fits for d and q also obey power laws, therefore data presented in figure 6 may be correlated with the following general expression: $h_L = d(\mathrm{Re}_L)(1-\lambda)^{q(\mathrm{Re}_L)}$, where $d(\mathrm{Re}_L) = e\,\mathrm{Re}_L^{\,r}$ and $q(\mathrm{Re}_L) = l\,\mathrm{Re}_L^{\,s}$.*

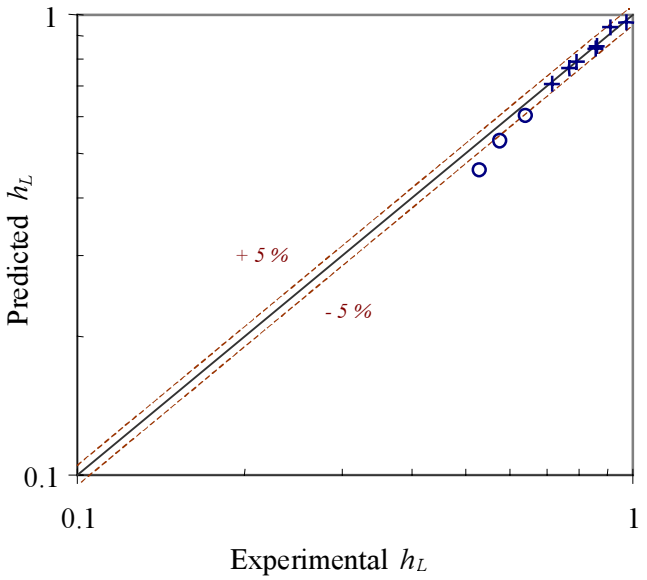

*Figure 8. Configuration **A**: Predicted liquid holdup h_L vs. experimental liquid holdup h_L for data and fittings presented in figures 6 and 7. Points denoted by ○ (open circles) correspond to the lowest liquid flow rate $Q_L = 0.2\ m^3/s$ in which we have short slugs separated by long regions of stratified flow (figure 5).*

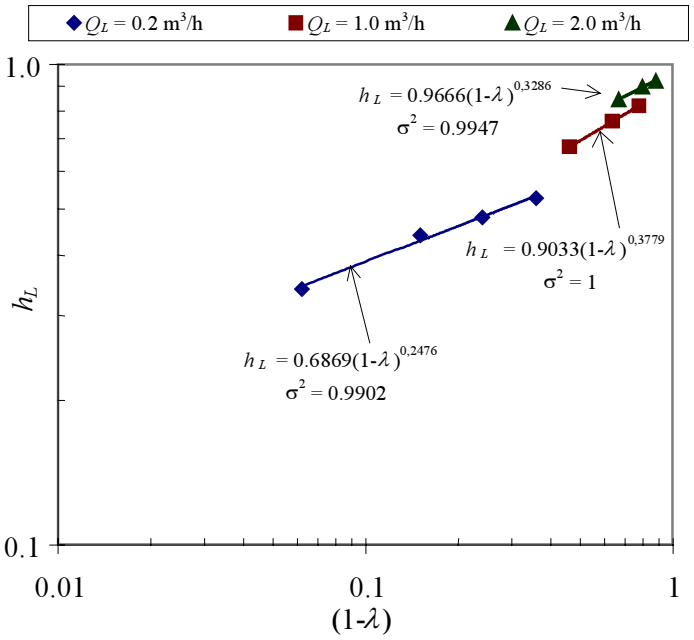

*Figure 9. Configuration **B**: Average liquid holdup h_L vs. the flow rate ratio $(1-\lambda)$, for different liquid flow rates Q_L, running air and oil in the tygon tube flow loop. To each liquid flow rate Q_L corresponds a liquid Reynolds number Re_L. A power law correlation of the form $h_L = d(1-\lambda)^q$ is obtained for each Re_L.*

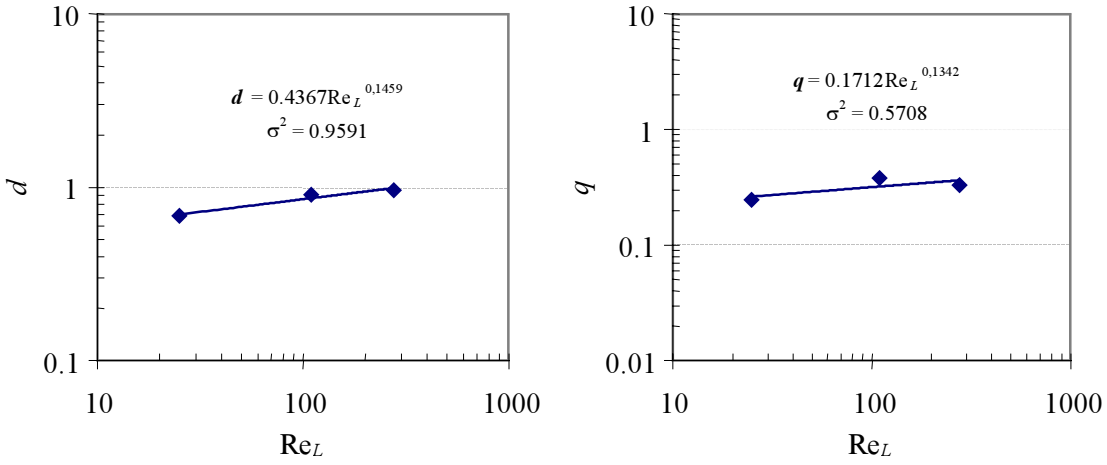

*Figure 10. Configuration **B**: Prefactor d and exponent q corresponding to the experimental data and fittings presented in figure 9 as a function of Re_L. Best fits for d and q also obey power laws, therefore data presented in figure 9 may be correlated with the following general expression: $h_L = d(\mathrm{Re}_L)(1-\lambda)^{q(\mathrm{Re}_L)}$, where $d(\mathrm{Re}_L) = e\,\mathrm{Re}_L^{\,r}$ and $q(\mathrm{Re}_L) = l\,\mathrm{Re}_L^{\,s}$.*

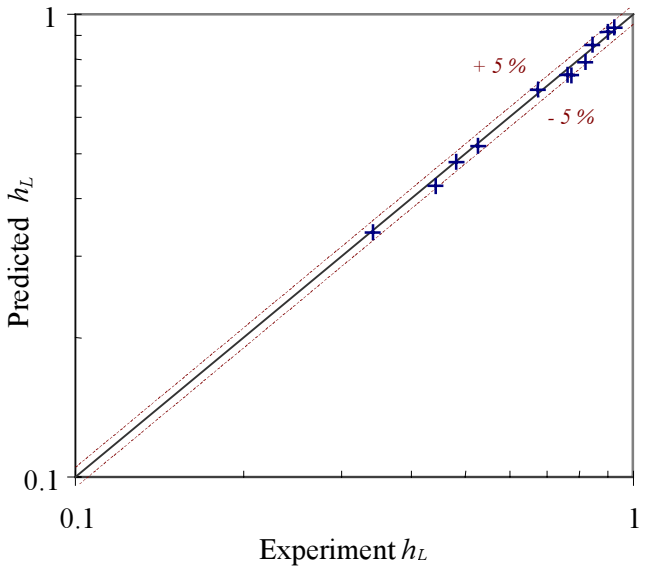

*Figure 11. Configuration **B**: Predicted liquid holdup h_L vs. measured liquid holdup h_L for data and fittings presented in figures 9 and 10. The error is less than 5%.*

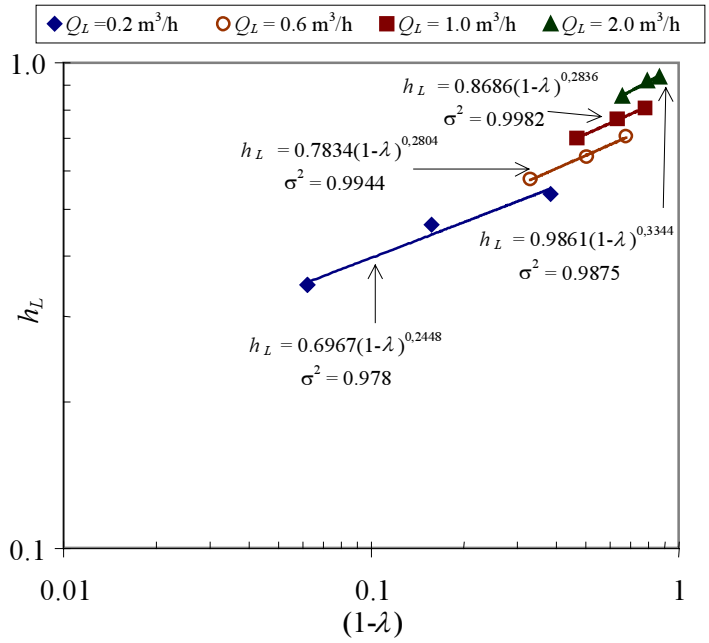

*Figure 12. Configuration **C**: Average liquid holdup h_L vs. the flow rate ratio $(1-\lambda)$, for different liquid flow rates Q_L. To each liquid flow rate Q_L corresponds a liquid Reynolds number Re_L. A power law correlation of the form $h_L = d(1-\lambda)^q$ is obtained for each Re_L.*

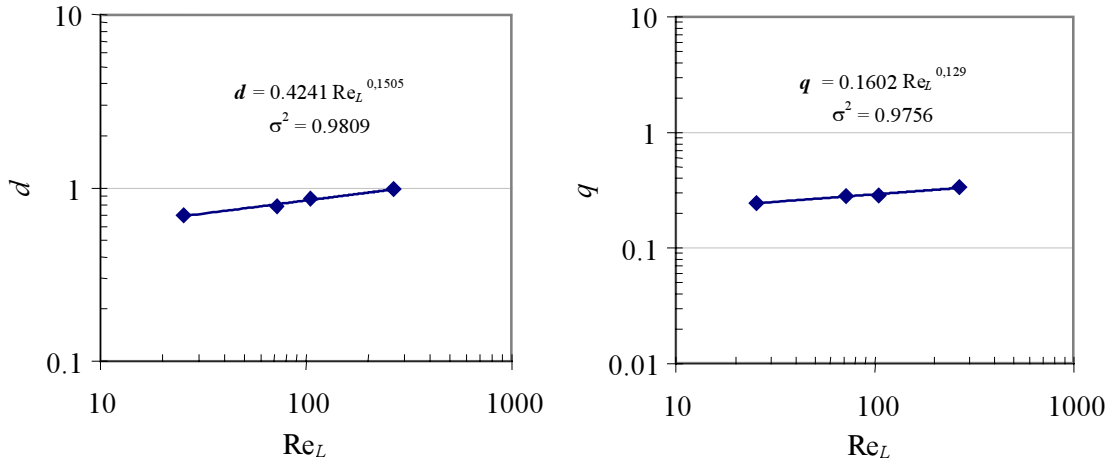

*Figure 13. Configuration **C**: Prefactor d and exponent q corresponding to the experimental data and fittings presented in figure 12 as a function of Re_L. Best fits for d and q also obey power laws, therefore data presented in figure 12 may be correlated with the following general expression: $h_L = d(\mathrm{Re}_L)(1-\lambda)^{q(\mathrm{Re}_L)}$, where $d(\mathrm{Re}_L) = e\,\mathrm{Re}_L^{\,r}$ and $q(\mathrm{Re}_L) = l\,\mathrm{Re}_L^{\,s}$.*

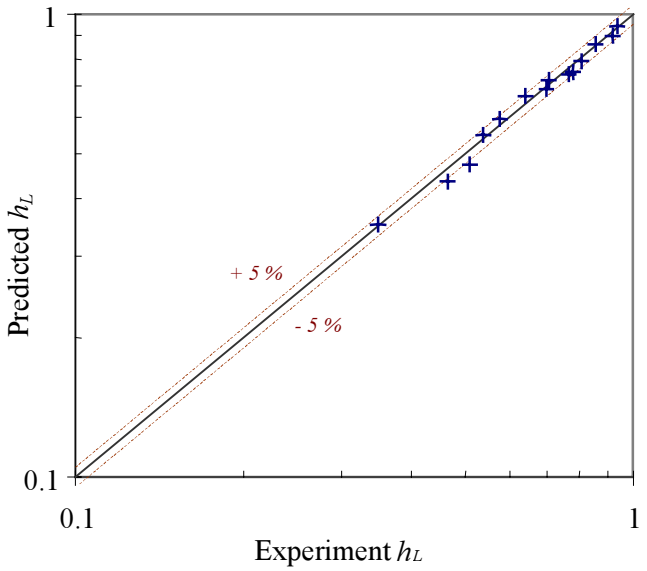

*Figure 14. Configuration **C**: Predicted liquid holdup h_L vs. measured liquid holdup h_L for data and fittings presented in figures 12 and 13. In general, the error is less than 5%.*

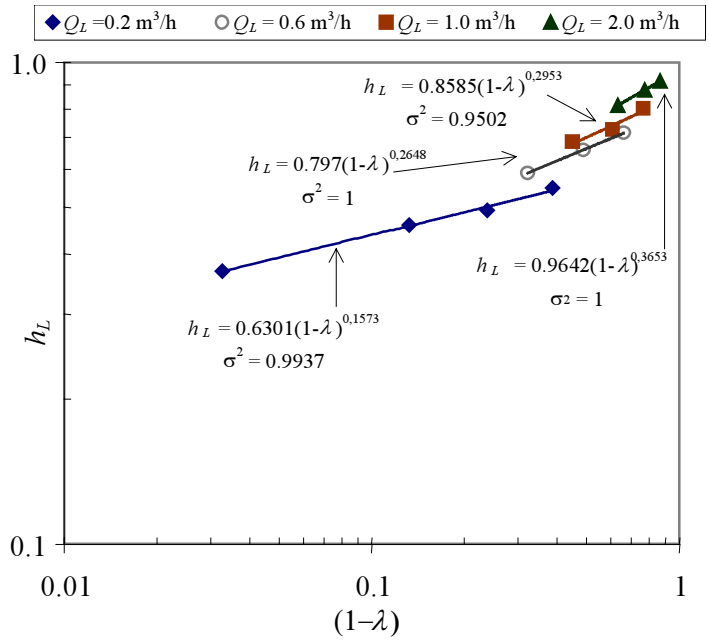

Figure 15. Configuration ***D****: Average liquid holdup h_L vs. the flow rate ratio $(1-\lambda)$, for different liquid flow rates Q_L, running air and oil in the tygon tube flow loop. To each liquid flow rate Q_L corresponds a liquid Reynolds number* Re_L*. A power law correlation of the form* $h_L = d(1-\lambda)^q$ *is obtained for each* Re_L*.*

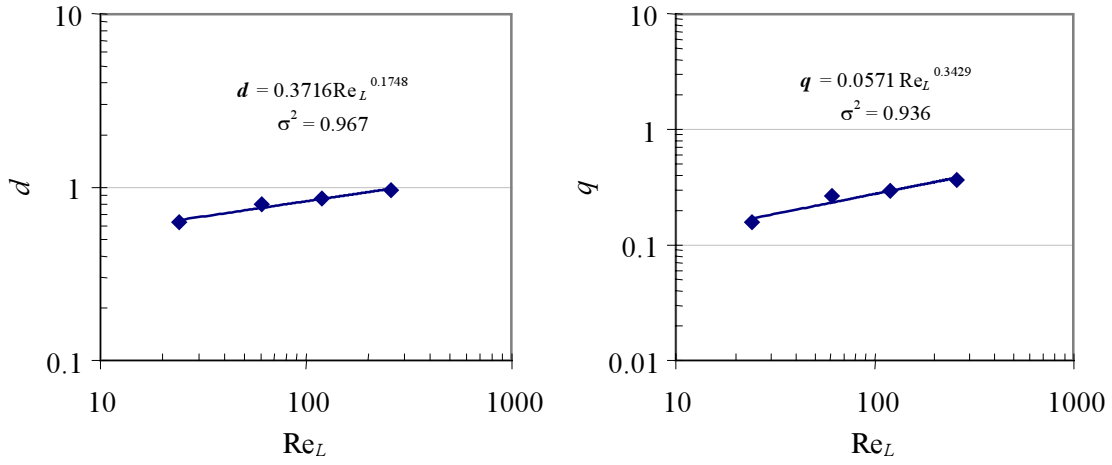

Figure 16. Configuration ***D****: Prefactor d and exponent q corresponding to the experimental data and fittings presented in figure 15 as a function of* Re_L*. Best fits for d and q also obey power laws, therefore data presented in figure 15 may be correlated with the following general expression:* $h_L = d(\mathrm{Re}_L)(1-\lambda)^{q(\mathrm{Re}_L)}$*, where* $d(\mathrm{Re}_L) = e\,\mathrm{Re}_L^{\,r}$ *and* $q(\mathrm{Re}_L) = l\,\mathrm{Re}_L^{\,s}$*.*

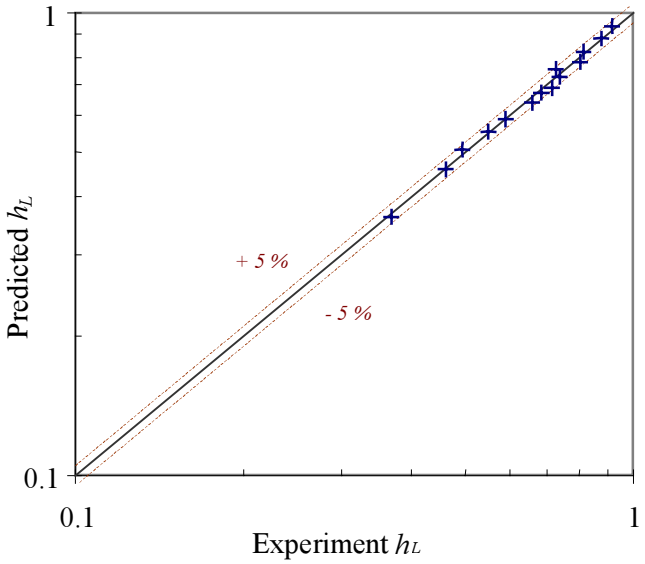

*Figure 17. Configuration **D**: Predicted liquid holdup h_L vs. measured liquid holdup h_L for data and fittings presented in figures 15 and 16. The error is less than 5%.*

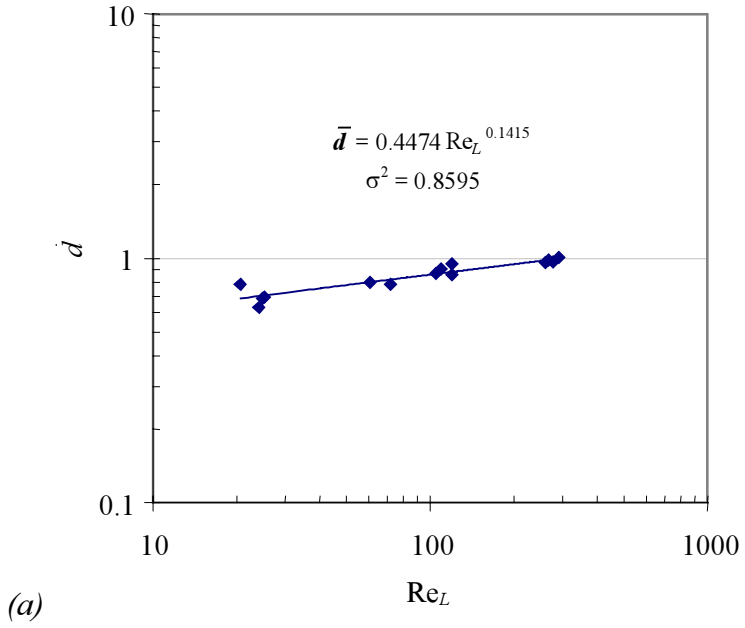

(a)

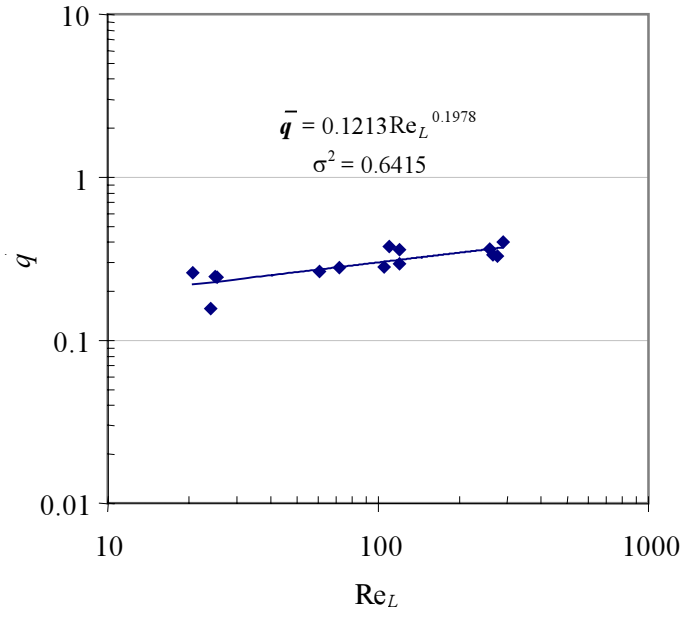

(b)

Figure 18. ALL Configurations: Prefactor d and exponent q corresponding to the experimental data and fittings presented in figures 6, 9, 12 and 15, as a function of Re_L*. Data points corresponds to all the studied configurations (**A** horizontal, **B**, **C** and **D**) and may be correlated with the following general expression:* $h_L = \bar{d}(Re_L)(1-\lambda)^{\bar{q}(Re_L)}$*, where* $\bar{d}(Re_L) = \bar{e}\, Re_L^{\bar{r}}$ *and* $\bar{q}(Re_L) = \bar{l}\, Re_L^{\bar{s}}$.

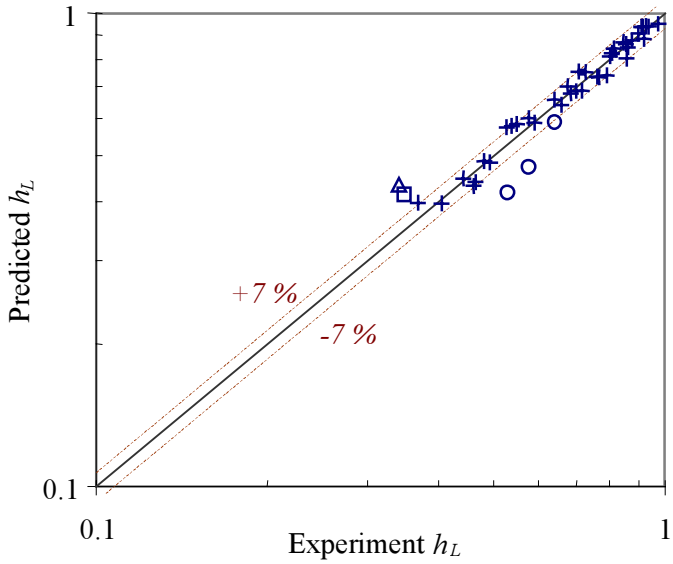

*Figure 19. ALL Configurations: Predicted liquid holdup h_L vs. measured liquid holdup h_L for data and fittings presented in figure 18. Data corresponds to all the configurations **A**, **B**, **C** and **D**. In general, the error is less than 7%, only predictions corresponding to $Q_L = 0.2$ m^3/s show errors up to 15% (experimental points denoted by open symbols (○, Δ and □ for the horizontal, **B** and **C** configurations, respectively).*

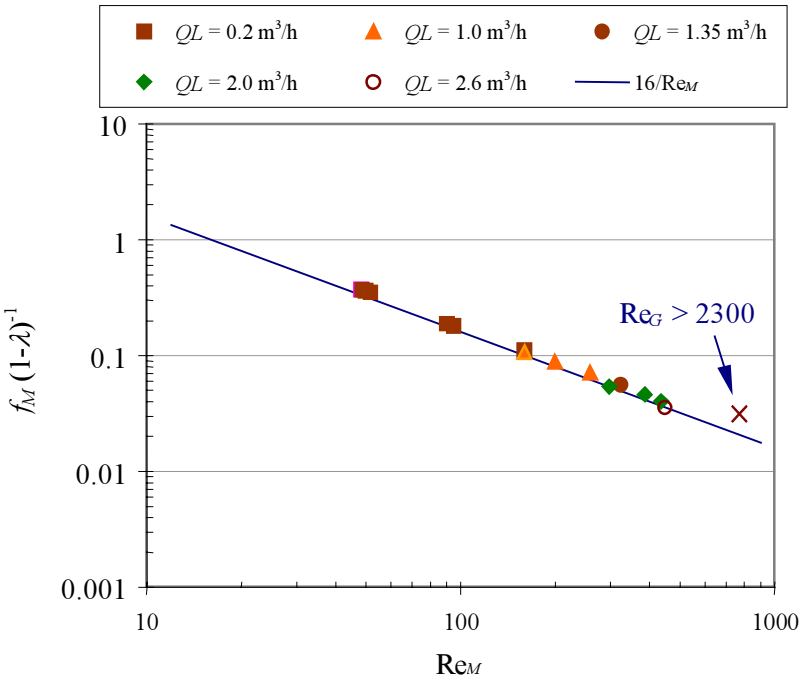

*Figure 20. Configuration **A** (horizontal): $f_M(1-\lambda)^{-1}$ vs. mixture Reynolds number Re_M, for different liquid flow rates Q_L, running air and oil in the tygon tube flow loop. The solid line corresponds to the curve $\frac{16}{\mathrm{Re}_M}$. Points denoted by × correspond to turbulent gas flow.*

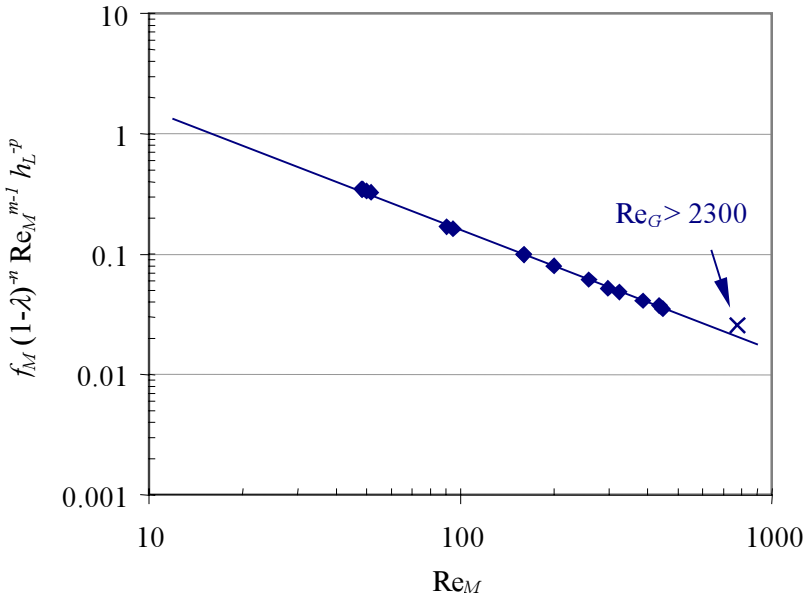

*Figure 21. Configuration **A** (horizontal): $f_M(1-\lambda)^{-n}\,\mathrm{Re}_M{}^{m-1}\,h_L{}^{-p}$ vs. mixture Reynolds number Re_M, for data presented in figure 20. The solid line corresponds to the curve $\frac{16}{\mathrm{Re}_M}$ (best fit).*

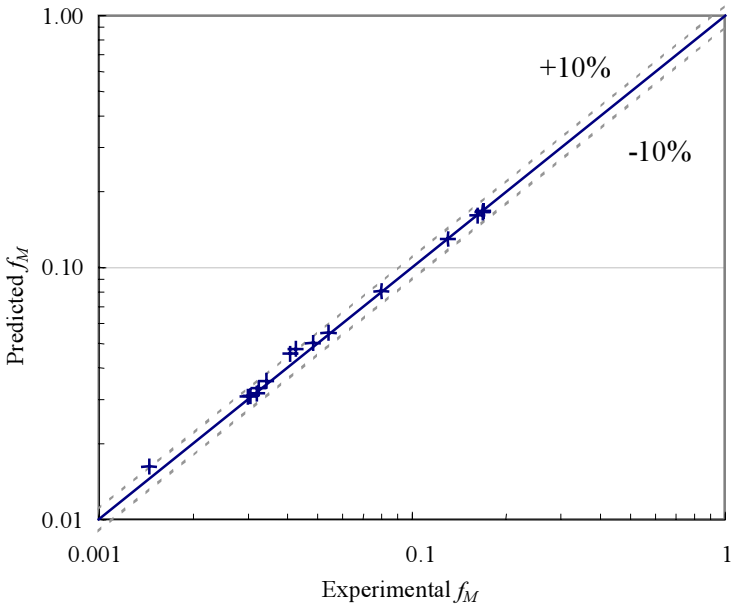

*Figure 22. Configuration **A** (horizontal): Predicted mixture Fanning friction factor f_M vs. the experimental mixture Fanning friction factor f_M, for the data and fitting presented in figure 21. The maximum absolute error is less than 10%.*

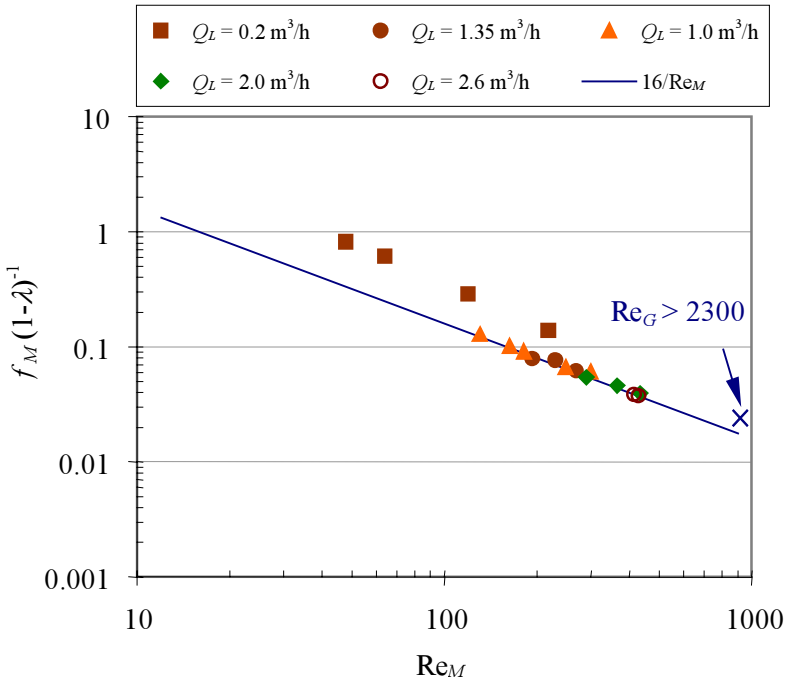

Figure 23. Configuration ***B:*** $f_M(1-\lambda)^{-1}$ *vs. mixture Reynolds number* Re_M *for different liquid flow rates* Q_L*, running air and oil in the tygon tube flow loop. The solid line corresponds to the curve* $\frac{16}{\mathrm{Re}_M}$*. Points denoted by* × *correspond to turbulent gas flow.*

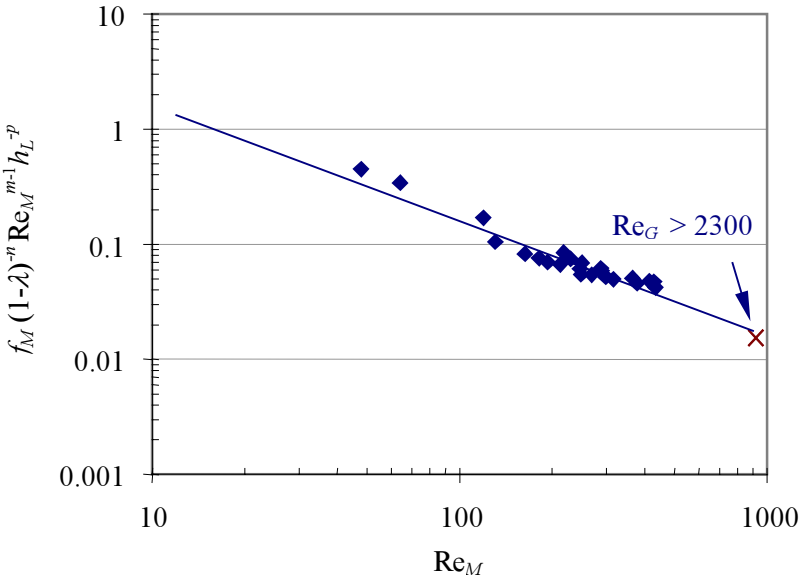

Figure 24. Configuration ***B:*** $f_M(1-\lambda)^{-n}\,\mathrm{Re}_M{}^{m-1}\,h_L{}^{-p}$ *vs. mixture Reynolds number* Re_M*, for data presented in figure 22. The solid line corresponds to the curve* $\frac{16}{\mathrm{Re}_M}$ *(best fit).*

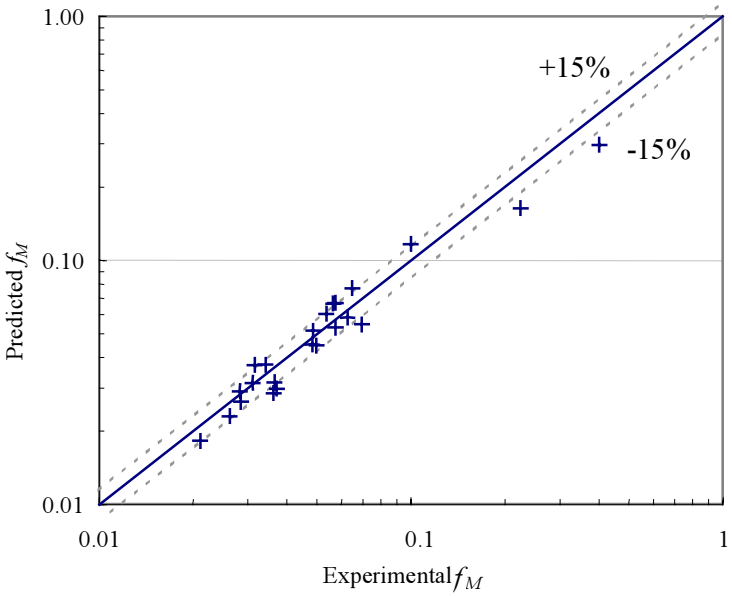

Figure 25. Configuration ***B:*** *Predicted mixture Fanning friction factor f_M vs. the experimental mixture Fanning friction factor f_M, for the data and fitting presented in figure 24. In general, the maximum absolute error is less than 15%.*

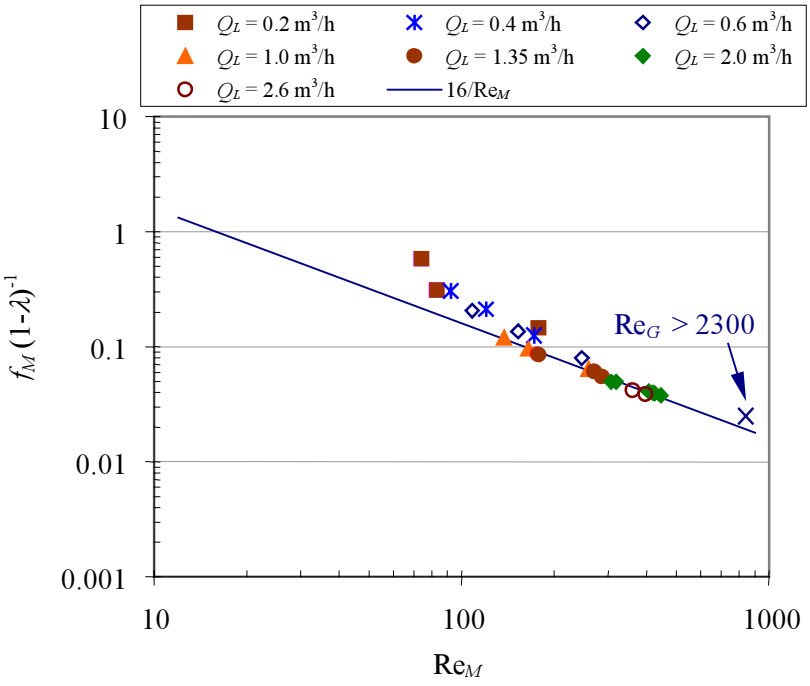

Figure 26. Configuration ***C:*** $f_M(1-\lambda)^{-1}$ *vs. mixture Reynolds number* Re_M *for different liquid flow rates* Q_L*, running air and oil in the tygon tube flow loop. The solid line corresponds to the curve* $\frac{16}{\mathrm{Re}_M}$*. Points denoted by × correspond to turbulent gas flow.*

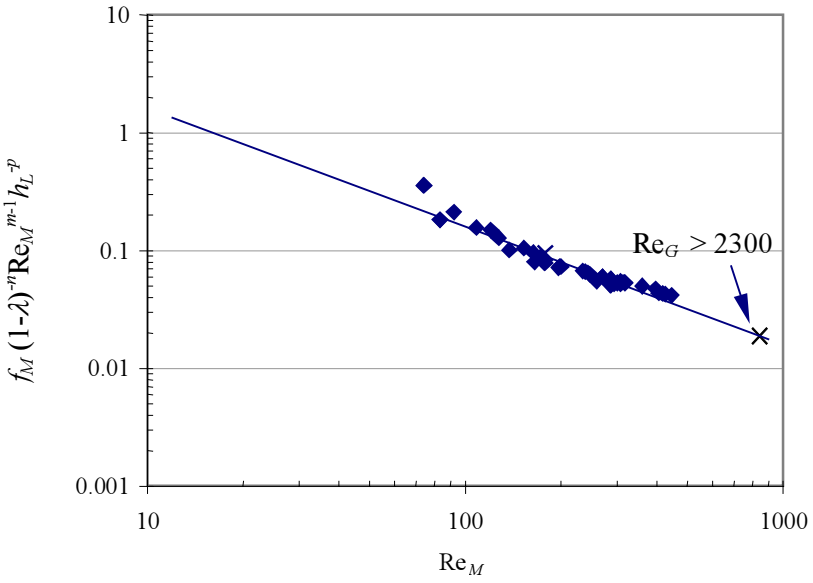

Figure 27. Configuration ***C:*** $f_M(1-\lambda)^{-n}\,\mathrm{Re}_M{}^{m-1}\,h_L{}^{-p}$ *vs. mixture Reynolds number* Re_M*, for data presented in figure 26. The solid line corresponds to the curve* $\frac{16}{\mathrm{Re}_M}$ *(best fit).*

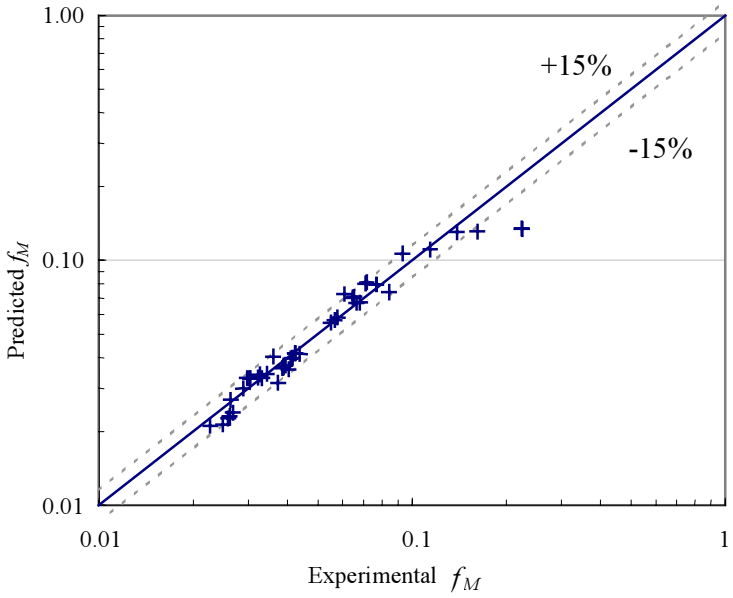

Figure 28. Configuration ***C:*** *Predicted mixture Fanning friction factor f_M vs. the experimental mixture Fanning friction factor f_M, for the data and fitting presented in figure 27. In general, the maximum absolute error is less than 15%*

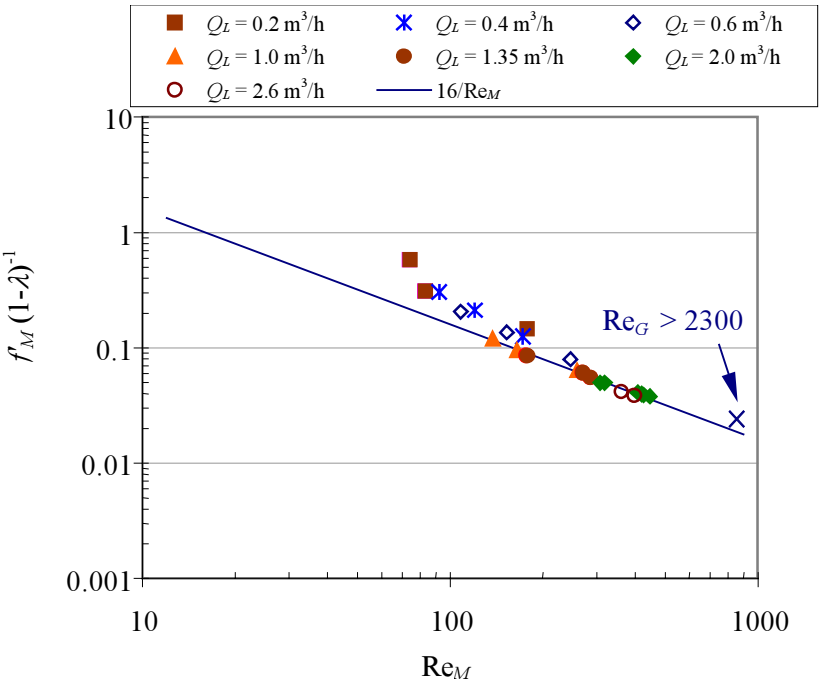

Figure 29. Configuration ***D:*** $f_M(1-\lambda)^{-1}$ *vs. mixture Reynolds number* Re_M *for different liquid flow rates* Q_L, *running air and oil in the tygon tube flow loop. The solid line* $\frac{16}{\mathrm{Re}_M}$ *corresponds to the curve. Points denoted by* × *correspond to turbulent gas flow.*

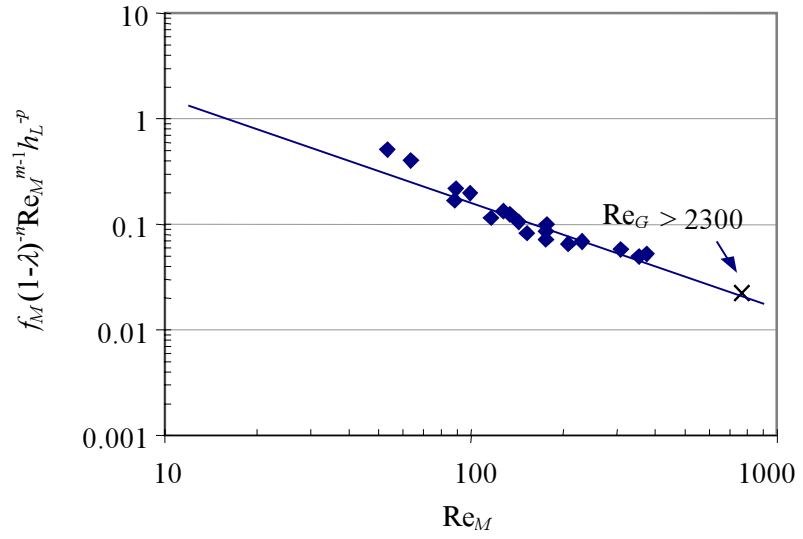

Figure 30. Configuration ***D:*** $f_M(1-\lambda)^{-n}\,\mathrm{Re}_M^{\,m-1}\,h_L^{\,-p}$ *vs. mixture Reynolds number* Re_M *for data presented in figure 29. The solid line corresponds to the curve* $\frac{16}{\mathrm{Re}_M}$ *(best fit).*

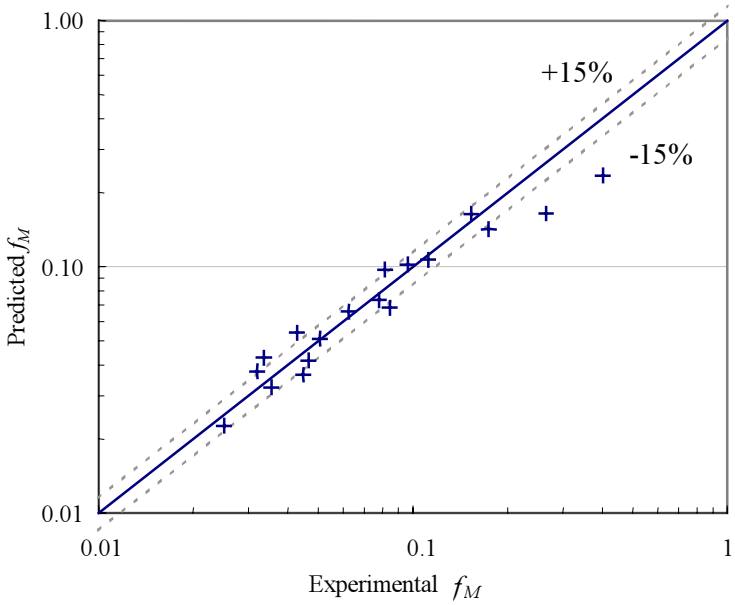

*Figure 31. Configuration **D:** Predicted mixture Fanning friction factor f_M vs. the experimental mixture Fanning friction factor f_M , for the data and fitting presented in figure 30. In general, the maximum absolute error is less than 15%.*

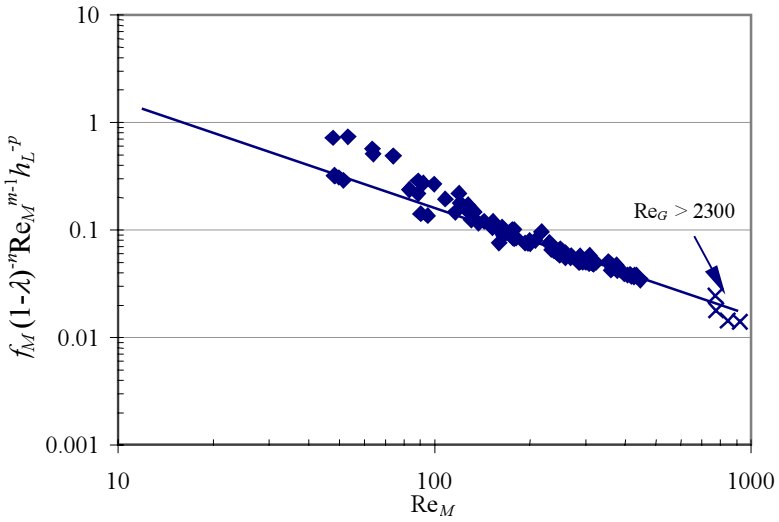

Figure 32. ALL Configurations: $f_M(1-\lambda)^{-n}\mathrm{Re}_M^{m-1}h_L^{-p}$ vs. Re_M for all data presented in figures 20, 23, 26 and 29. In this case p = 0.024 is nearly zero and the correlation for the friction factor is nearly independent of holdup.

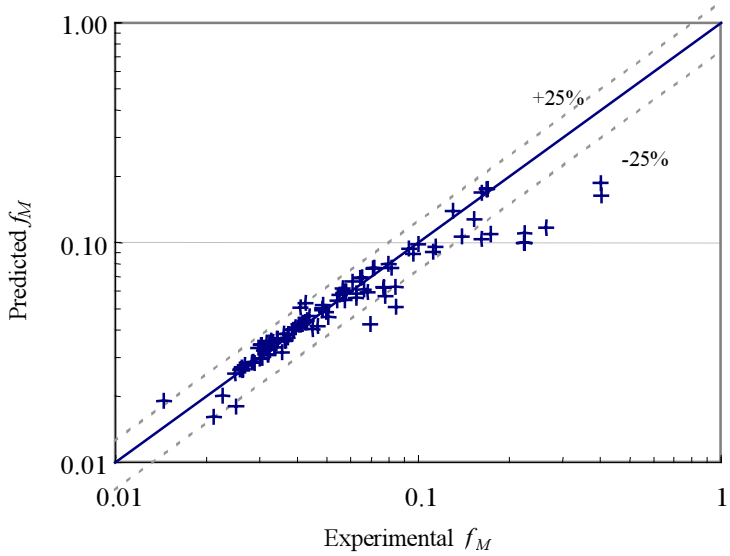

Figure 33. ALL Configurations: Predicted mixture Fanning friction factor vs. experimental friction factor for data presented in figure 32. In general the error is less than 25%.